Destriping Cosmic Microwave Background Polarimeter data

A. Zonca[a,*], B. Williams[a], P. Meinhold[a], P. Lubin[a]

[a]Department of Physics, University of California, Santa Barbara
Santa Barbara, CA 93106

Abstract

Destriping is a well-established technique for removing low-frequency correlated noise from Cosmic Microwave Background (CMB) survey data. In this paper we present a destriping algorithm tailored to data from a polarimeter, i.e. an instrument where each channel independently measures the polarization of the input signal.

We also describe a fully parallel implementation in Python released as Free Software and analyze its results and performance on simulated datasets, both the design case of signal and correlated noise, and with additional systematic effects.

Finally we apply the algorithm to 30 days of 37.5 GHz polarized microwave data gathered from the B-Machine experiment, developed at UCSB. The B-Machine data and destriped maps are made publicly available.

The purpose is the development of a scalable software tool to be applied to the upcoming 12 months of temperature and polarization data from LATTE (Low frequency All sky TemperaTure Experiment) at 8 GHz and to even larger datasets.

Keywords: cosmic background radiation, methods: data analysis, instrumentation: polarimeters

1. Introduction

The destriping technique (Kurki-Suonio et al., 2009; Keihänen et al., 2010; Ashdown et al., 2007; Delabrouille, 1998; Maino et al., 2002; Natoli et al., 2001; Revenu et al., 2000; Poutanen et al., 2006) is widely used in the CMB field for removing correlated low-frequency noise, typically due to thermal drifts, amplifiers gain fluctuations and changes in atmospheric emission. To be effective, destriping requires that the data are acquired with a scanning strategy (Dupac and Tauber, 2005) which assures frequent crossing points, i.e. looking at the same sky location at different times.

Correlated noise at low frequency is often modeled as $1/f$ noise:

$$P(f) \propto \sigma^2 \left[1 + \left(\frac{f_k}{f} \right)^{\alpha} \right], \qquad (1)$$

where:

- f is the frequency,

- the knee frequency f_k denotes the frequency where white and correlated noise contribute equally to the total noise

- the power spectrum below the knee frequency is increasing as a power law with exponent α.

For a typical survey experiment, making multiple passes over the same region of sky, destriping can efficiently remove 1/f noise with a knee frequency lower than the scan rate by removing a sequence of offsets (called baselines) of a predetermined length, typically of order the scan length (or spin period). The baselines are estimated iteratively by binning the data on a sky map and minimizing the scatter among different measurements of each pixel.

The destriping algorithm allows the removal of the correlated noise with minimal impact on the signal (Efstathiou, 2005; Maino et al., 1999). Destriping can be thought of as a high-pass filter that only affects the noise in the timestream.

This paper first introduces (Sec. 2) the B-Machine experiment (Williams, 2010) to highlight the features of a CMB polarimeter and the typical data processing required to convert raw data to calibrated timelines ready for map-making and noise characterization. Sec. 3 de-

*Corresponding author
    Email addresses:* `zonca@deepspace.ucsb.edu` (A. Zonca),
`brianw@deepspace.ucsb.edu` (B. Williams),
`peterm@deepspace.ucsb.edu` (P. Meinhold),
`lubin@deepspace.ucsb.edu` (P. Lubin)

scribes in detail the destriping technique, a Maximum Likelihood algorithm for removing low frequency correlated noise from the data. We describe in detail the implementation specifics in Sec. 4 for application of destriping to a polarimeter and present results of the destriping on simulated data in Sec. 5. Sec. 6 is dedicated to the application of destriping to B-Machine data, analyzing the impact of destriping in map, frequency and angular power spectrum domain.

The B-Machine experiment itself and the data analysis pipeline presented in this work are focused on preparing the upcoming LATTE (Low frequency All sky TemperaTure Experiment) experiment.

LATTE is a ground based telescope designed to survey the diffuse microwave foregrounds, primarily from the Milky Way. Its main purpose is to help fill the gap in the data that exists between the 408 MHz Haslam (Haslam et al., 1982) survey and the lowest WMAP band at 23 GHz (Gold et al., 2011). The data from LATTE will be useful for the study of the CMB by better characterizing foreground emission so that they can be more effectively removed from WMAP and Planck (Planck Collaboration et al., 2013) data. But it will also add to our understanding of the Inter Stellar Medium (ISM) (Spitzer Jr, 2008), in particular spinning dust emission (Planck Collaboration et al., 2011) and Galactic haze (Dobler and Finkbeiner, 2008; Planck Collaboration, 2013).

LATTE will have a single detector with a 30% bandwidth centered at 8 GHz (future plans include bands in the 3 to 15 GHz range) and an angular resolution of about 2°, it will be based on cryogenically cooled radiometers to measure relative sky temperature and polarization with an expected sensitivity as low as 340 μK $\sqrt{s}$. For comparison the C-Bass (King et al., 2010) 5 GHz radiometer, an experiment with similar scientific goals, has a bandwidth of 1.4 GHz and a sensitivity of about 580 μK $\sqrt{s}$.

2. Polarimeters data

B-Machine is a prototype ground-based CMB polarimeter operated at White Mountain Research Station in California during 5 months in 2008, see Table 1 for a summary of the experiment features, and the instrument paper (Williams, 2010) for a detailed description.

The key enabling technology of the B-Machine polarimeter is a reflection half-wave plate rotating at 30 Hz, located between the primary and the secondary mirrors of our 2 m Gregorian telescope. The wave plate continuously rotates the polarization of the incoming

Table 1: Summary of B-Machine.

Frequency	37.5 GHz
Beam full width half max	22.2 arcmin
Number of horns	4
Scanning strategy	45° elevation, 70s revolution
Sensitivity (I)	$16, 16.4, 23.1, 5.3$ mK/ $\sqrt{\mathrm{Hz}}$
Sensitivity (Q, U)	$7.6, 6.7, 10.5, 2.8$ mK/ $\sqrt{\mathrm{Hz}}$
$1/f$ noise knee frequency in Q and U	5.0 mHz
Amount of valid data	314, 329, 30, 293 hours
Altitude	3800 m
Atmosphere temperature	10 K

waves. Viewing the sky through this wave plate, the radiometer is sensitive to a linear polarization state which rotates 120 times per second, and this measurement can be demodulated to completely solve for the linear polarization state of the incoming radiation.

In detail, for each disk rotation, each polarimeter outputs a measurement for q and one for u, i.e. the Q and U Stokes polarization states in the reference frame of the telescope. These timestreams need then to be rotated to the Equatorial or Galactic Q and U using the known pointing and orientation information.

Demodulation has also the effect of highly suppressing the gain fluctuations of the receiver, effectively being equivalent to chopping 4 times per revolution, i.e. 120 Hz, with a reference target. Although B-Machine detectors were designed as pure polarimeters, it is possible also to measure the intensity I of the incoming signal by integrating the signal across the disc rotation. However, without modulating and then demodulating I is strongly affected by correlated noise and difficult to use for scientific purposes. For the LATTE experiment we are including a high-frequency switch that allows switching between the sky and a reference target to provide a performance comparable to the polarized channels.

A complete absolute calibration with a reference target was performed only twice, at the beginning and at the end of the campaign. Data were calibrated to physical units with a daily relative calibration.

Data were sampled at 33.4 Hz, but, due to bad samples or operational issues in the instrument, they show several gaps. There are two primary reasons we decided

to remove flagged samples and to fill the gaps with white noise:

- Noise characterization requires computing Fast Fourier Transforms (FFTs), which generally require constant sampling frequency. Flagged samples need to be replaced by white noise.

- The destriper, for ease of implementation, does not use timing information but just a fixed number of samples per offset, i.e. 2000, therefore it assumes a constant sampling rate.

Our white-noise filling algorithm just replaced all flagged and missing samples with gaussian white noise with the same mean and standard deviation of the good samples for each day of data.

Pointing reconstruction and calibration outputs consist of about 3 GB of data for each channel, containing:

- timing information

- pointing angles

- bad data flags

- I, q and u measurements calibrated to physical units [K].

3. Algorithm

B-Machine temperature and polarization outputs are fully decoupled, because the polarimeter measures q and u directly, and binning over a full revolution to measure temperature effectively removes any polarized emission and gives a pure I component. Map-making can be therefore performed independently on the temperature and polarization outputs; temperature-only destriping and IQU destriping of polarization-sensitive detectors are already well described in the literature (Kurki-Suonio et al., 2009; Ashdown et al., 2007; Delabrouille, 1998; Maino et al., 2002; Revenu et al., 2000; Poutanen et al., 2006), in the following section we will focus on the specifics of destriping for polarimeters, i.e. QU only destriping.

Destriping models the output of each of the two channels of a polarimeter as:

$$y = (R_Q P m_Q + R_U P m_U) + n, \qquad (2)$$

where:

- y is the data timeline, an array of length n_t, already calibrated in physical units [K]

- m_Q , m_U are the Q and U component maps pixelized using the HEALPix[1] scheme, each of length n_{pix}

- P is the pointing matrix, a $[n_t, n_{pix}]$ sparse matrix with one element equal to 1 for each row corresponding to the pixel pointed by the detector in that sample. Therefore Pm is the scanning of the map to a timeline, given the pointing embodied in P. The pointing matrix is the same for both channels of each horn,

- n is the white plus correlated noise timeline.

For polarization sensitive detectors, it is also necessary to rotate the polarized QU components in the detector reference frame. This is accomplished by the diagonal $[n_t, n_t]$ matrices R_Q, R_U where each element takes into account the current orientation of the detectors. Given the measured parallactic angle[2] ψ, R_Q and R_U definition depends whether the channel is q or u polarization:

$$q \, \text{channel} : R_Q[t, t] = \cos(2\psi[t]) \qquad (3)$$
$$R_U[t, t] = \sin(2\psi[t]) \qquad (4)$$
$$u \, \text{channel} : R_Q[t, t] = -\sin(2\psi[t]) \qquad (5)$$
$$R_U[t, t] = \cos(2\psi[t]), \qquad (6)$$

where t is the sample index or sample time. Of course in the implementation those diagonal matrices can just be stored as an array of length n_t and multiplied element-wise to the Pm timeline.

The noise timeline can be separated in two components:

$$n = Fa + w, \qquad (7)$$

a white noise component w and a correlated component modeled by the baselines array a of length n_b multiplied by the $[n_t, n_b]$ sparse matrix F. Each row of F has only one nonzero element, equal to 1, at the column corresponding to the baseline which includes the current sample. Therefore the matrix repeats each of the elements in a by the baseline lengths and outputs an array of length n_t.

Substituting Eq. 7 in Eq. 2 the complete model is:

---

[1]HEALPix website:`http://healpix.jpl.nasa.gov`
[2]The parallactic angle ψ is the angle between the direction of polarization sensitivity of the detector and the meridian passing by the current pointing direction

$$y = (R_Q Pm_Q + R_U Pm_U) + Fa + w. \qquad (8)$$

First we can compute the hitmap, the map which contains the number of hits for each pixel, as:

$$h = P^T P. \qquad (9)$$

Using Maximum Likelihood analysis (Kurki-Suonio et al., 2009), we can compute the map m, given the baselines a:

$$m_Q = h^{-1} P^T \left[R_{Qq}(y_q - Fa_q) + R_{Qu}(y_u - Fa_u) \right] \qquad (10)$$

$$m_U = h^{-1} P^T \left[R_{Uq}(y_q - Fa_q) + R_{Uu}(y_u - Fa_u) \right]. \qquad (11)$$

In this equation, first we remove the $1/f$ noise from y_q and y_u by subtracting the given baselines, then the signal is projected by the R matrices to the sky reference frame. Noise weighting is not necessary because we are building each horn map independently, and we assume noise stationarity. Then the P_T matrix sums all the observations into the two maps, typically called sum maps, which are then divided by the hitmap h to average the observations.

In QU polarimeter map-making, each pixel is by design measured simultaneously by the q and u channels, therefore the weighting process is simpler than in the polarization-sensitive radiometer IQU map-making case where instead it is necessary to invert a $[3, 3]$ matrix.

Both Eq. 10 and Eq. 11 can be rewritten by merging the binning operation in a single matrix B:

$$m = B(y - Fa) \qquad (12)$$

where:

$$B = h^{-1} \tilde{P}^T R$$

$$\tilde{P} = \begin{bmatrix} P & \\ & P \end{bmatrix}$$

$$R = \begin{bmatrix} R_{Qq} & R_{Uq} \\ R_{Qu} & R_{Uu} \end{bmatrix}$$

Replacing Eq. 10 and Eq. 11 in the Maximum Likelihood equation and solving instead for the baselines, we get the destriping equation:

$$\left[\tilde{F}^T \left(I - R\tilde{P}B \right) \tilde{F} \right] a = \tilde{F}^T \left(I - R\tilde{P}B \right) y \qquad (13)$$

where:

$$\tilde{F} = \begin{bmatrix} F & \\ & F \end{bmatrix}$$

$$y = \begin{bmatrix} y_q \\ y_u \end{bmatrix}$$

$$a = \begin{bmatrix} a_q \\ a_u \end{bmatrix}.$$

The matrix $R\tilde{P}B$ rescans the binned map created by B to a timeline, therefore the matrix $I - R\tilde{P}B$ removes the estimated signal from the timeline, and then the F^T matrix bins it for each baseline period. The right hand side of the destriping equation performs signal removal on the input data y, and the residual is summed over for each baseline period; the final result is an array of length n_b that contains the residual noise averaged by baseline. The left hand side performs exactly the same operation but on the timeline $\tilde{F}a$, i.e. the timeline composed just of the baselines, which are the unknowns in this equation.

The purpose of a destriper is to find the baseline array that produces the same residual noise of the data over each baseline period. The left-side matrix of the destriping equation is a dense matrix of size $[n_b, n_b]$, and even for modest datasets it is computationally too heavy to be inverted, and typically it is never explicitly computed, either; iterative solvers like Conjugate Gradient (CG) (Shewchuk, 1994) or Generalized Minimal RESidual method (GMRES) (Saad and Schultz, 1986) allow to estimate the baselines with the required accuracy by just applying algorithmically the steps needed to apply the left-hand operator, without involving any large matrix operation.

4. Implementation

B-Machine itself is a prototype experiment, built to test the design of the polarization rotator and to explore the challenges of a ground based polarimeter. A similar approach has been taken for the software design, the purpose is to implement a data analysis pipeline that works for the current dataset but is ready to be extended for future experiments, where the amount of data is going to be orders of magnitude larger. Also, we release this software publicly under GNU GPL License[3], so that it may be studied and used by other scientists. Therefore we have reviewed many of the available technologies and chosen those most promising to be applied to large datasets. We focused in particular to the most standard and robust technologies, favoring simplicity and maintainability over pure performance.

---

[3]http://www.gnu.org/licenses/gpl.html

4.1. Data storage

HDF5 is the most widespread file format for new applications in the scientific community (The HDF Group, 2000-2010), as it allows binary machine independent hierarchical data to be stored efficiently on disk and supports parallel reading and writing through MPI(Gabriel et al., 2004). Nowadays the HDF5 C, C++, Fortran libraries are installed in nearly every supercomputer, and can also easily be installed on desktops. HDF5 software is definitely complex, because it allows extremely flexible data selection and format conversion of multi-dimensional datasets, but still it is one of the easiest options for high performance parallel I/O.

4.2. Parallel linear algebra

The key element for the implementation of the destriper is the choice of a distributed linear algebra package, the most popular packages in the scientific community are PETSc[4] by Argonne National Laboratories (Balay et al., 1997) and Trilinos[5] by Sandia National Laboratories (Heroux et al., 2005). Both are implemented in C++ and provide implementation of distributed arrays through MPI and several solvers for linear and non-linear systems. We favored Trilinos because the APIs are more modular, fully Object Oriented, therefore easier to work with.

4.3. Programming language

Trilinos is implemented in C++ and has a native Python interface named PyTrilinos, built on top of NumPy. PyTrilinos offers an interface to the underlying C++ objects with minor performance degradation, as both the communication and the math operations are executed by the optimized C++ library. We implemented the Python destriper dst, which implements data distribution using Epetra (Trilinos package), data loading using HDF5, GMRES solver using Belos (Trilinos package), and cython[6] for two computationally intensive functions.

4.4. MPI communication strategies

Data, baselines and maps are distributed uniformly among the available processors, each process has a local map which involves just the pixels (HEALPix) hit by its own section of the data, therefore the same pixels are duplicated in several processes. When the destriping algorithm requires the application of the matrix P^T first the data are binned locally on each process, then the local maps are distributed and summed to the global map which has unique pixels and that is distributed uniformly among the processes, independently from the local map. This process is automatically performed by Trilinos with highly optimized communication strategies, it is just necessary to specify the source and target distributions. Typically the map is weighted and then rescanned to time domain, therefore the opposite operation is performed, where the pixel values from the global unique map are distributed to all the local maps and overwrite the previous value. Then rescanning to time domain is simply a local operation.

4.5. Access to the code

The full source code is available on github, `http://github.com/zonca/dst`, under GNU GPL Free Software license. The software is designed to destripe any dataset in HDF5 format which provides I, q and u data and pointing information in the correct format, and outputs hitmaps, binned maps, destriped maps and baseline arrays.

5. Simulations

All maps in the next sections are projected with a Mollweide projection. Since B-Machine covers about 50% of the sky, we have sliced the full sky view focusing on the observed area, a full sky image in Galactic coordinates is available in Fig. 13.
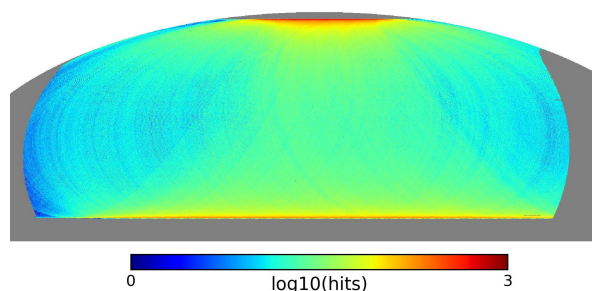

Figure 1: Base 10 logarithm of the hitcount map for B-Machine channel 6 in Equatorial coordinates at HEALPix N_{side} 512, i.e. a pixel area of 47.2 square arcminutes for about 30 days of observing time.

We have produced a set of test data using the same pointing information of one of the B-Machine channels

---

[4]`http://www.mcs.anl.gov/petsc/`
[5]`http://trilinos.sandia.gov/`
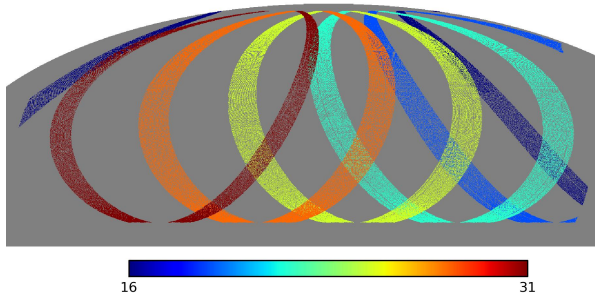[6]`http://www.cython.org`

Figure 2: B-Machine scanning strategy for one night of acquisition: each ring displays the pixels covered by one hour of data, about 51 revolutions at 70 seconds per revolution, from 16, i.e. hits between 16:00 and 17:00, to 31, i.e. hits between 7:00 and 8:00, every 3 hours, i.e. the second ring is 19:00 to 20:00. Crossings between different rings provide leverage to the destriping algorithm for solving the baselines.

and simulated timelines of growing complexity. Sky coverage is about 44.8%; on a HEALPix N_{side} 512 pixelization, i.e. resolution of about 6.9′, the median hitcount per pixel is 20, with higher hitcount toward the North Pole and the Equator, see a channel hitcount map in Fig. 1.

Fixed elevation scanning (45°) at 1 revolution each 70 seconds gives good coverage and frequent crossings near the North pole and the Equator in the Equatorial reference frame. Fig. 2 illustrates the scanning strategy for August 9th, 2008; each ring plots the covered pixels for one hour acquisition time, we plotted a ring each 3 hours, at 16:00, 19:00, 22:00, 1:00, 4:00 and 7:00 in local time, from right to left, i.e. from 16:00 in blue to 31:00 (7:00) in red. The sections of the data nearby sunrise and sunset were contaminated by large thermally induced gain variations and were masked out.

The input signal was based on WMAP 7 years Q band, smoothed by 1° in order to reduce the noise in map domain; white noise variance and $1/f$ noise knee frequency and slope were based B-Machine channel 6 noise properties.

The choice of the baselines length is typically related to the spinning frequency of the experiment, a baseline length of about the length of a scanning ring helps a more uniform distribution of the crossing points, which are the key to a successful solution of the destriping equations. B-Machine spins around its vertical axis in about 70 seconds, therefore we chose a baseline length slightly shorter, of about 60 seconds, i.e. 2000 samples at 33.4 Hz.

Signal only simulations show that the destriper solves for null baselines, up to the machine precision of 10^{-16}, as expected by the fact that the input signal has been generated itself by a map and therefore all measurements on the same pixel have a consistent signal. Other tests involved white noise only or $1/f$ noise only simulations.
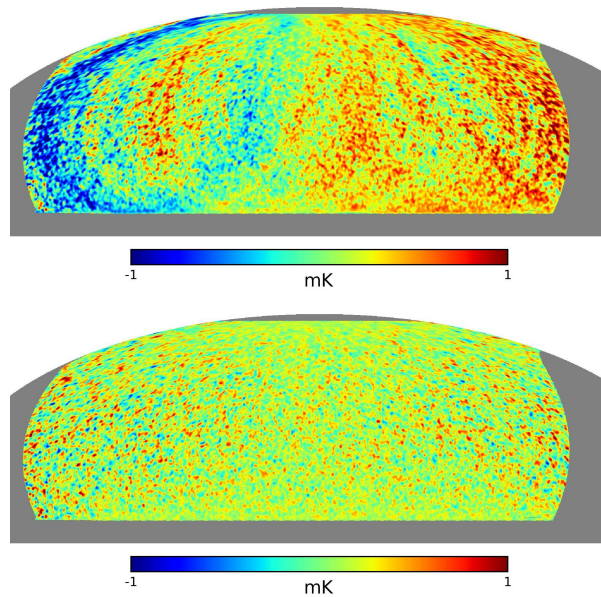

Figure 3: Difference between binned (top) and destriped (bottom) simulated maps and the input signal, smoothed with a 1° gaussian beam. The simulations were based on WMAP signal and simulated $1/f$ noise. Destriping removes the stripes caused by correlated noise, residuals are consistent with white noise

The most interesting simulation involves signal, $1/f$ and white noise, in this case we have computed the residual maps by removing the input signal from the output maps; the difference between the input signal and the output before destriping (top of Fig. 3) smoothed by 1°, is dominated by stripes caused by correlated noise. After removing the baselines from the timestream and produced the destriped maps (bottom of Fig. 3), the measurement is not affected by any stripe, but dominated by white noise. The amplitude of the residual white noise is modulated by the hits per pixels and agrees with the hitmap in Fig. 1.
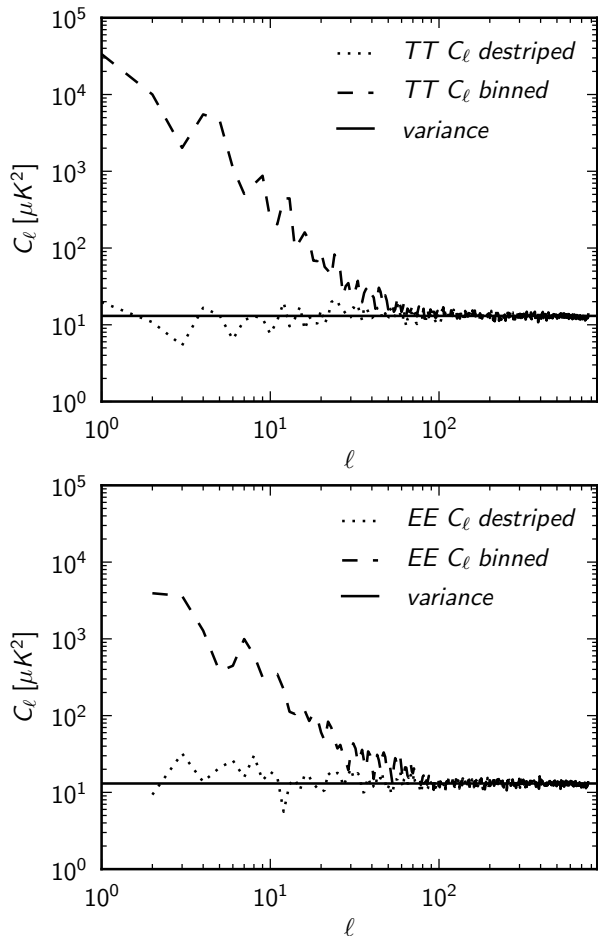
Figure 4: *TT* and *EE* angular power spectra of the noise in the binned and destriped maps of the simulation of signal and $1/f$ noise based on B-Machine scanning strategy and noise properties. Destriping completely removes correlated noise both in temperature and polarization, the residual angular power spectrum after destriping agrees with the expected level computed from the variance of pure white noise.

Fig. 4 shows the spherical harmonic transforms of the binned and destriped map residuals compared to the expected noise due to the instrument white noise: destriping effectively removes all the low frequency power due to $1/f$ signal and retrieves a measurement just dominated by white noise, both in temperature and in polarization. The reduced χ^2 of the residual map drops from 1.052 for *I* and 1.026 in *Q* in the binned map to 1.0002 for *I* and 1.0012 for *Q* in the destriped map.

Other sources of systematic effects that cannot be modeled as $1/f$ noise with a knee frequency lower than the spin frequency are not affected by the destriping al-

gorithm, and need to be dealt with before applying destriping. In the rest of the section we will show two illustrative examples of these types of systematics effects which can affect B-Machine and show their impact on the destriping algorithm. Since such systematics are instrument-specific and vary largely, we do not try to be exhaustive or general.

Gain variations of the instrument are multiplicative effects, and are not efficiently corrected for by a destriping algorithm. Actually the destriping algorithm in such scenario can be harmful, as it spreads the effect of the uncorrected gain error to a larger area of the map. We created a signal-only simulation with a 10% uncorrected gain fluctuation on a day timescale, modeled as a sinusoidal effect with maximum at noon and minimum at midnight. B-Machine observed from 5pm to 8am, therefore most of the gain error shows up as a negative residual in the map, stronger on the galactic plane. The destriping algorithm in this case tries to correct the gain error by solving for negative baselines, however this mainly has the effect of creating rings of spurious signals that affect the whole sky circle that crosses the brightest regions of the galaxy, see the top right part of Fig. 5. Results in *Q* and *U* are similar, but not as dramatic due to the much lower foreground emission. This simulation is a worst case scenario, because this effect can be mitigated by aggressively masking the galactic emission.
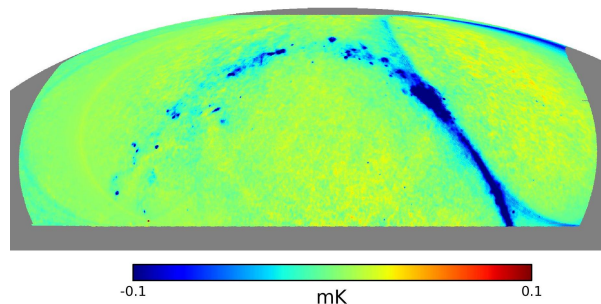

Figure 5: *I* map of a signal-only simulation with uncorrected 10% gain fluctuation on a daily timescale, the destriper solves for spurious baselines on the rings that cross the brightest regions of the galaxy.

Another sort of systematic effects are spin-synchronous effect, typical examples for ground-based instruments are Radio Frequency Interference (RFI) signals from ground emitters, e.g. radio transmitters, radars, or satellites, e.g. geostationary telecommunication satellites. RFI signals have typically a fixed azimuth, or more often 2 fixed azimuths, in the local
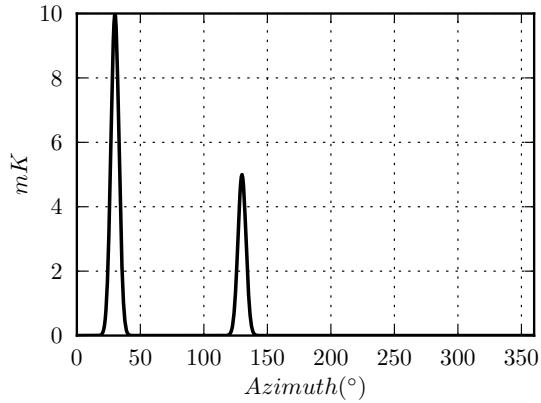
Figure 6: Model for a spin-synchronous RFI signal affecting two directions fixed in the local reference frame, 30° and 130° with a peak height of 10 and 5 mK and a FWHM of 80′
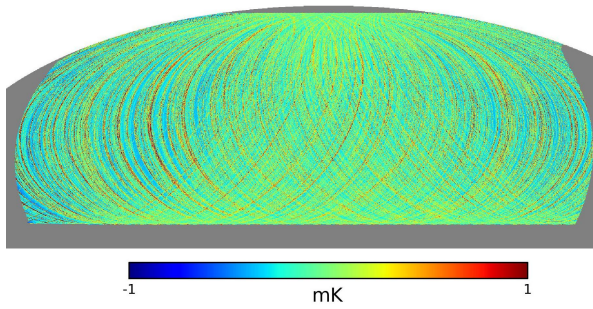

Figure 7: I map of a signal-only simulation with a spin-synchronous RFI signal (model in Fig. 6); the destriper is unable to remove correlated noise on timescales shorter than the baseline length

rected for in time-domain before running map-making, gain variations need to be modeled with a proper calibration process, RFI effects should be removed either using a template fit or with convolution of the beam side lobes with the source.

reference frame, when the source signal enters the telescope from directions other than the main field of view, i.e. stray-light on the often annular beam side lobes.

We created a simple model of a RFI signal with two gaussian peaks with a Full Width Half Max (FWHM) of twice the B-Machine FWHM, separated by 100° and with an amplitude of 10 and 5 mK, see Fig. 6. The effect of RFI in frequency domain is to add correlated noise on timescales equal and shorter than the spin frequency, which cannot be removed by the destriper. Both the binned and the destriped map (Fig. 7) show residual stripes distributed uniformly across the sky with an amplitude of the order of 1 mK; destriping has no significant impact on the maps. Both effects should be cor-

8

6. Destriping B-Machine data

The dataset size after cleaning is between 35 and 40 million samples for I, q and u for each polarimeter, with the exclusion of channel 3 where hardware issues caused about 90% of the data to be invalid. In the following section we present the results of map-making on channel 6 of B-Machine, which is the best channel both for noise characteristics and impact of systematic effects.

6.1. Temperature maps

The B-Machine I channel was not designed for scientific exploitation, it is just a secondary output of the polarimeter, it does not benefit from the modulation/demodulation and is therefore affected by $1/f$ noise over the spin frequency, which cannot be efficiently removed by the destriper.

The binned I map (Fig. 8a) is dominated by significant white noise due to the short integration time per pixel, and by large systematic effects due to temperature gradients on the experiment. Fig. 8c shows the map after destriping, and Fig. 8b the difference between the binned and the destriped map, i.e. the baselines binned to the sky. It is evident that the destriping algorithm manages to remove most of the large gradients due to day-night temperature drift.

However, two different types of systematics are still visible in the map:

- stripes all over the sky, oriented along the scanning rings are likely due to the tail of $1/f$ over the spin frequency, which has a similar effect to the spin-synchronous RFI simulated in Sec. 5, Fig.7

- broader features, like the hot bands on the top of the map, are likely due to uncorrected gain drifts, similar to the result displayed in Fig.5.

Nevertheless, Milky Way emission and at least two compact sources, M42 and the Crab Nebula are visible in the map, see the full sky map in Galactic coordinates in Fig. 13 at the end of the paper.

6.2. Polarization maps

The q and u polarimeter outputs are affected by large offsets due to the electronics that need to be either removed by high-pass filtering the data, or they can just be dealt with by the destriper itself, that can better constrain their value by using the crossing points.
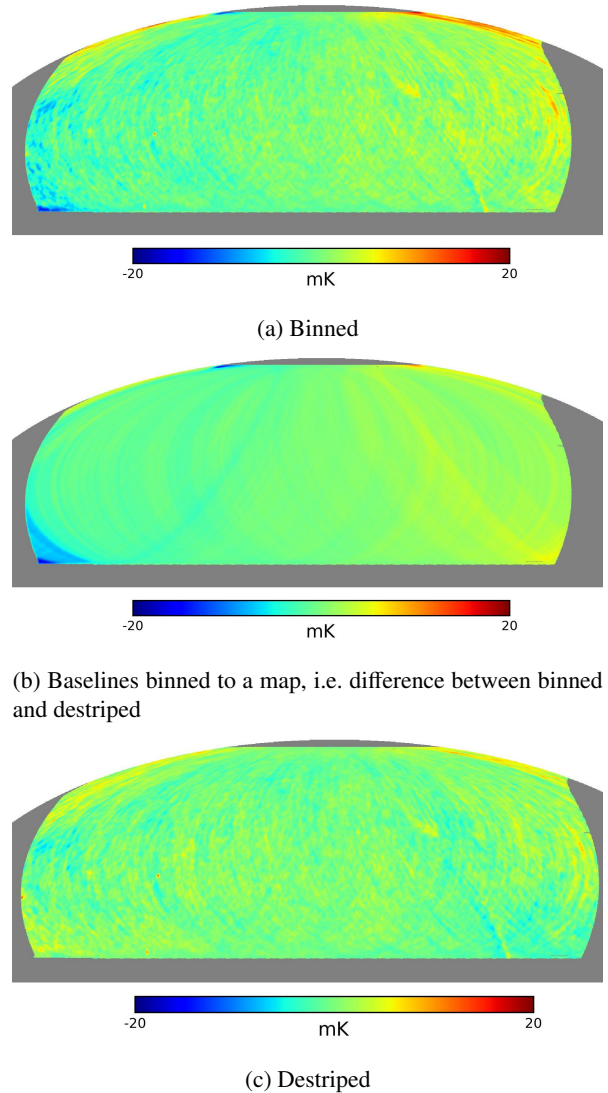

(a) Binned

(b) Baselines binned to a map, i.e. difference between binned and destriped

(c) Destriped

Figure 8: B-Machine channel 6 I maps for about 30 days of acquisition in Equatorial reference frame, smoothed with a 1° gaussian beam. The destriping algorithm removes from the naively binned map Fig. 8a the solved 1 minute long baselines, which can be projected to the sky as Fig. 8b, to achieve the destriped map Fig. 8c. Fig 8c in Galactic coordinates is available in Fig. 13.
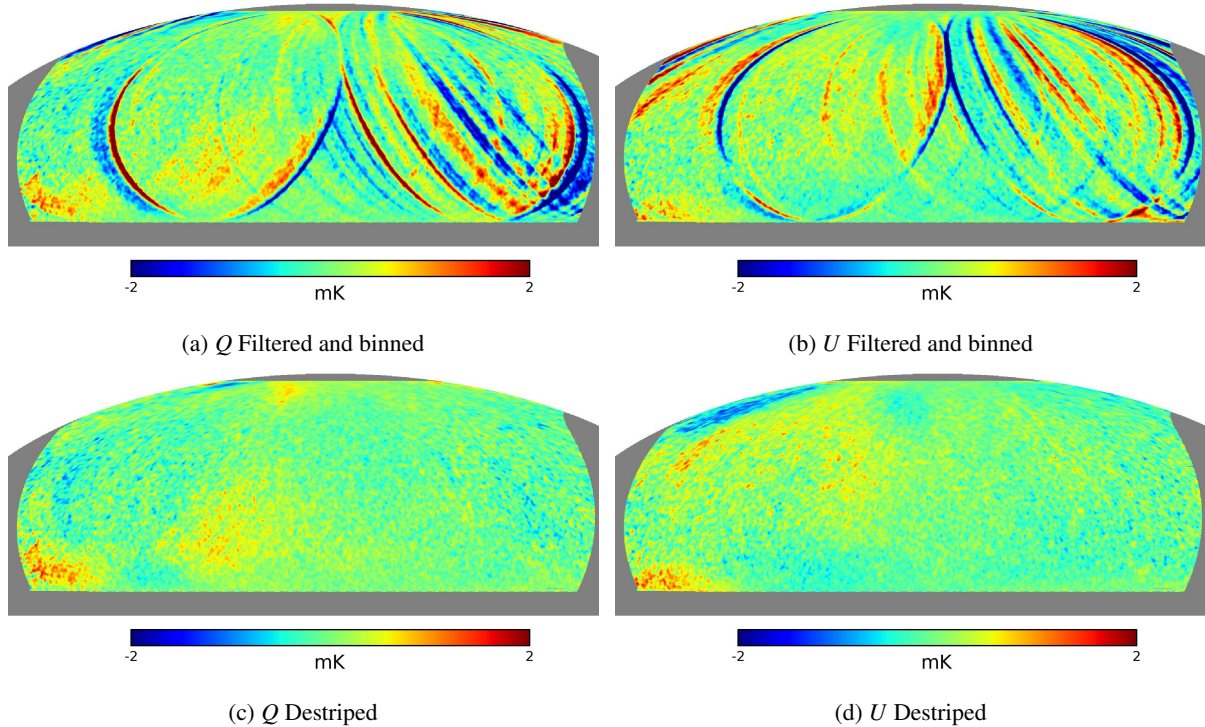
(a) *Q* Filtered and binned

(b) *U* Filtered and binned

(c) *Q* Destriped

(d) *U* Destriped

Figure 9: B-Machine channel 6 *Q* and *U* maps in Equatorial coordinates smoothed with a 1° gaussian beam, Fig. 9a and Fig. 9b were produced by filtering the data with a Butterworth high pass filter with a cut-off at 1 hour and then directly binning to a map. Fig. 9c and Fig. 9d are the results of the destriping algorithm with 1 minute long baselines.

A direct binning of polarized data would be completely dominated by their offsets, therefore a more interesting comparison is achieved by first high-pass filtering the data with a 8th order Butterworth filter with a cut-off of 1 hour. The filter successfully removes the offsets but leaves several large stripes due to thermal gradients, see Fig. 9a and Fig. 9b. Those features are removed instead by the destriper, see Fig. 9c and Fig. 9d. Moreover, filtering the data might also have an impact on the sky signal, effectively modifying the transfer function of the instrument.

However, the high white noise and few artifacts probably due to calibration cause large scale residuals. In particular the hot blob at the bottom left is due to gain drift caused by the rising Sun. The white noise level in the map is however too high to detect diffuse synchrotron emission from the Milky Way, the only visible object is Tau A, the Crab Nebula.

Maps in HEALPix FITS format are publicly available on the Internet via Figshare[7] (Zonca)[8]. A sample time-line of 3 days is available on the same data repository, access to the full timelines is available upon request.

6.3. Point sources

Tau A (Crab Nebula) is the only point source that is visible in the *Q* destriped map, and it has been used for calibration and pointing reconstruction purposes. Its flux agrees with WMAP Q-band (Weiland et al., 2011) at the level of 20% in *I* and 6% in *Q*. Tau A emission in *U* is instead too faint to be detected in the data.

Fig. 10a, Fig. 10b and Fig. 10c show *IQU* gnomonic projection 5° patches around Tau A of destriped maps at N_{side} 512 and smoothed with a gaussian beam of 40′. Fig. 10d, Fig. 10e and Fig. 10f show the difference between binned maps (after high-pass filtering) and destriped maps. The destriping process has a negligible impact on *I* maps, because the source emission is over 20 times higher than the residual $1/f$. In the *Q* polarization map, destriping is efficiently removing stripes due to correlated noise of the same order of magnitude of the source flux.
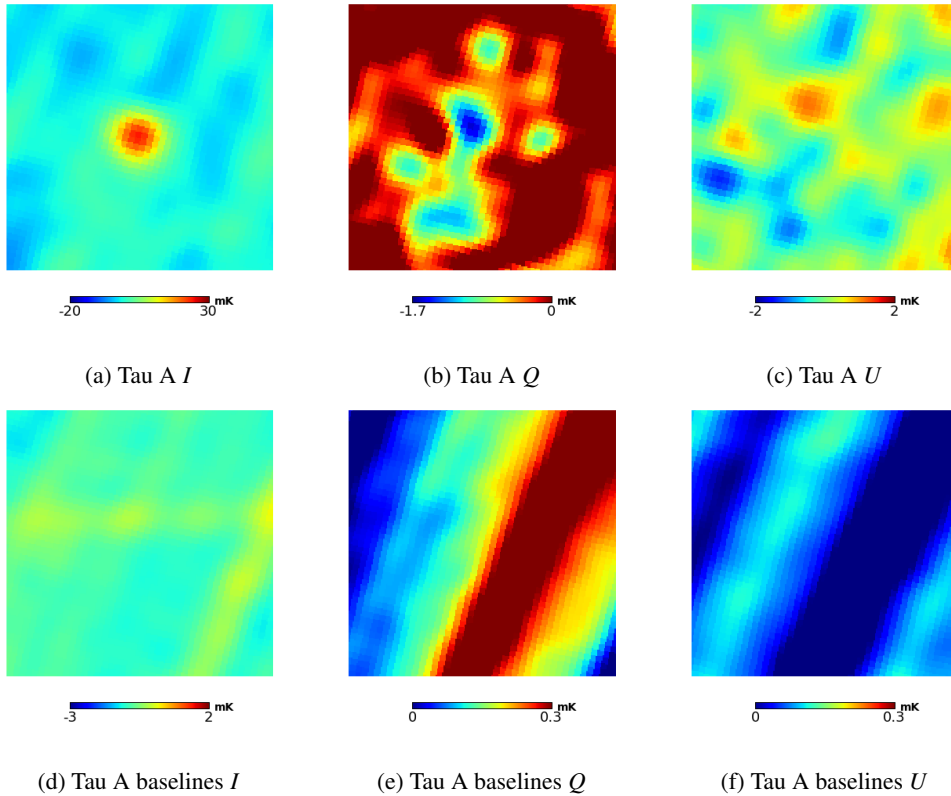
---

[7]http://www.figshare.com
[8]http://dx.doi.org/10.6084/m9.figshare.644507

Figure 10: Tau A (Crab Nebula) N_{side} 512 maps for channel 6 smoothed with 40′ gaussian beam , **top row**: IQU maps, emission in I and Q agrees with WMAP, emission in U is lower and is not detected in the B-Machine maps. **Bottom row**: difference between binned maps (after filtering) and destriped maps. Destriping in I has a negligible effect on strong sources, while in polarization it is essential to be able to identify the sources.

6.4. Noise characterization

In the following section we will review the impact of destriping on the properties of the noise in the data in frequency and angular power spectrum domain.

6.4.1. Frequency domain

B-Machine has very different noise properties for the temperature and the polarization channels; q and u channels have a low knee frequency thanks to the 120 Hz chopping provided by the Polarization rotator, while the I channel has significant correlated noise over the spinning frequency (~1/70 Hz).

Fig. 11 shows the effect of destriping on the timelines, i.e. the comparison between the signal y and the baseline removed signal $y - Fa$, the $1/f$ noise below the baseline length of 60 seconds is correctly removed in the polarized channels. In the temperature channel, instead, the high tail of the spectrum still suffers from correlated noise, i.e. does not show the white noise plateau; moreover, at low frequencies, the shape of the noise does not

agree with a $1/f$ spectrum that is one of the assumptions for the design of the destriping algorithm. Still it is useful to apply destriping to the data to remove slower correlated noise from the timelines.

This is an extreme case for the application of a map-making algorithm, typically building an instrument with no correlated noise on timescales shorter than the spinning frequency is a strong design driver, which pushes either to increase the spinning frequency or more often employ strategies to improve the noise properties of the detectors, e.g. fast-switching with a reference target. In the B-Machine case the focus was only on polarization, so the I channel was not designed for scientific purposes.

6.4.2. Angular power spectrum

Analyzing the angular power spectrum of the destriped maps allows us to check the consistency of the map noise with the noise level predicted by the noise properties of the receivers. Given a white noise stan-
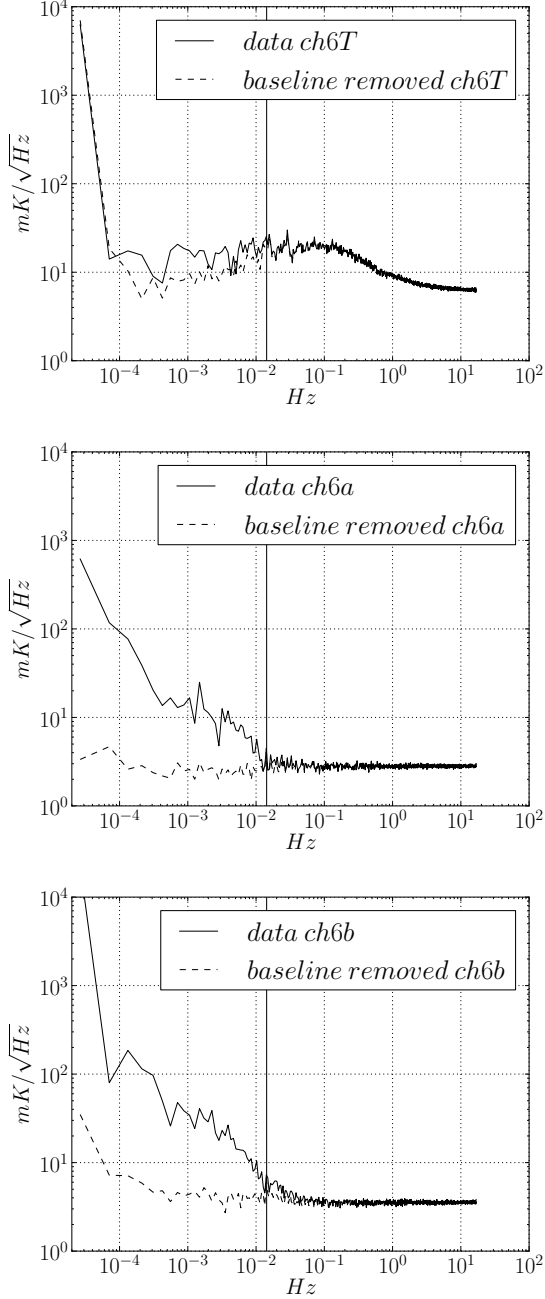
Figure 11: Channel 6 *I*, *q* (`ch6a`) and *u* (`ch6b`) data amplitude spectra before and after destriping for 1 day of data; the spectrum has been averaged over bins of linearly increasing length.

dard deviation of σ, we can estimate the expected noise level in the angular power spectrum as:

$$C_\ell = \Omega_{\text{pix}} \langle \frac{\sigma^2}{\tau} \rangle = \Omega_{\text{pix}} \langle \frac{\sigma^2 f_{\text{samp}}}{hits} \rangle, \qquad (14)$$

where Ω_{pix} is the pixel area and τ the integration time, i.e. the ratio between the sampling frequency and the hitcount map.

Fig. 12 shows the *EE* and *BB* angular power spectrum of the Channel 6 destriped maps extracted from the *Q* and *U* data, in comparison with the binned maps of filtered data, spectra were computed on partial sky using HEALPix `anafast` and then corrected by the sky fraction to achieve the equivalent spectra for a full-sky map. We just compare maps on the same sky cut, therefore we do not need a more refined analysis that corrects for the correlation across angular scales (Wright et al., 1994).

The large scale features in the destriped maps after smoothing, Fig. 9d and Fig. 9c, strongly affect the power spectrum at low multipoles ($\ell < 100$), even increasing the mask to about half of the available sky. Still some residual systematic effects impact the largest scales, probably due to gain drifts, but the effect of destriping is evident at intermediate scales ($50 < \ell < 200$) and the power spectrum agrees with the predicted white noise variance down to $\ell = 250$. As explained in Sec. 5, correcting for multiplicative effects like gain drifts is outside of the scope of a destriper and the data needs to be properly calibrated before map-making. This could not be achieved in B-Machine, but in LATTE we plan to better monitor the thermal environment and apply a continuous calibration based on thermal sensors measurements. Moreover, the *I* channel in LATTE will have noise properties comparable to the polarization channels, and we plan to use the CMB dipole to provide another calibrator for the experiment.
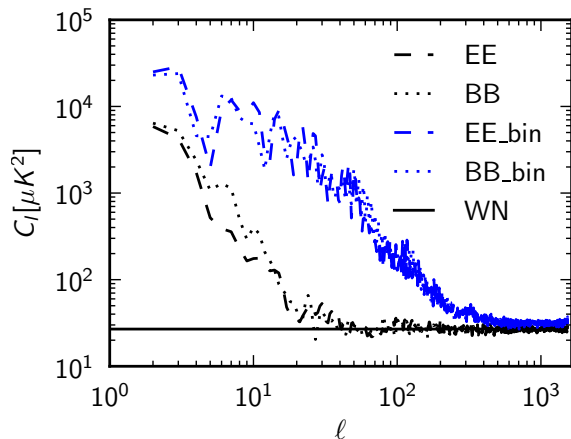
Figure 12: Angular power spectrum of Channel 6 N_{side} 512 binned and destriped maps, corrected for the sky fraction. We compare in blue the *EE* and *BB* spectra of the filtered and binned maps to the black spectra of the destriped maps, adding also as a reference a solid black line with the expected white noise floor. Destriping removes excess power at intermediate scales $(50 < \ell < 200)$ due to $1/f$ noise, but cannot correct for large scale features caused by uncorrected gain fluctuations in the data.

7. Test on 1 year of data

In order to assess the scalability of `dst` to larger datasets, we created a simulated dataset with the same setup used in the validation tests for a longer time span, about 12 months of data. We ran `dst` on this dataset using the Gordon supercomputer, located in the San Diego Supercomputing center; Gordon was designed for data-intensive applications, which is suitable for the destriping algorithm, which has no CPU-intensive operations and is typically memory-limited. We configured the test run to make use of 16 MPI processes, the destriping phase required 80 GMRES iterations to reduce the residual by a factor of 10^{12} and took 6 minutes.

This performance figure is a positive result considering that the software has been designed for simplicity and robustness and not for speed. In the future, specific sections of the code can be optimized leading to a significant boost in performance. For example currently data are read from HDF5 files in serial mode, which is definitely going to be the most likely bottleneck for larger applications, therefore one of the first improvements could be in implementing a parallel version. It is going to be easy now that `h5py` has native support for the parallel version of HDF5.

8. Conclusion

We have outlined a destriping algorithm tailored at polarimeters data, and described its parallel implementation in `Python` based on `Trilinos` for communication and `HDF5` for data storage. We showed the results of the software on a simulated dataset and on the B-Machine 37.5 GHz data, analyzing its impact in time-domain, in map-domain and in spherical harmonics domain.

The destriping algorithm is effective in removing correlated noise due to additive effects like thermal fluctuations both in temperature and polarization data. In presence of other systematic effects, like gain variations or spin-synchronous effect, destriping can be ineffective of even harmful, they therefore need to be dealt with before the map-making stage.

The software implementation is targeted to the upcoming LATTE experiment, expected to provide about 12 months of temperature and polarization data at 8 GHz (about half billion samples), and can easily be further optimized for larger datasets. Both the code and the data are made available to the scientific community under Free Software licenses.

References

Ashdown, M.A.J., Baccigalupi, C., Balbi, A., Bartlett, J.G., Borrill, J., Cantalupo, C., de Gasperis, G., Górski, K.M., Hivon, E., Keihänen, E., Kurki-Suonio, H., Lawrence, C.R., Natoli, P., Poutanen, T., Prunet, S., Reinecke, M., Stompor, R., Wandelt, B., Planck CTP Working Group, 2007. Making sky maps from Planck data. AAP 467, 761–775. doi:10.1051/0004-6361:20065829, arXiv:arXiv:astro-ph/0606348.
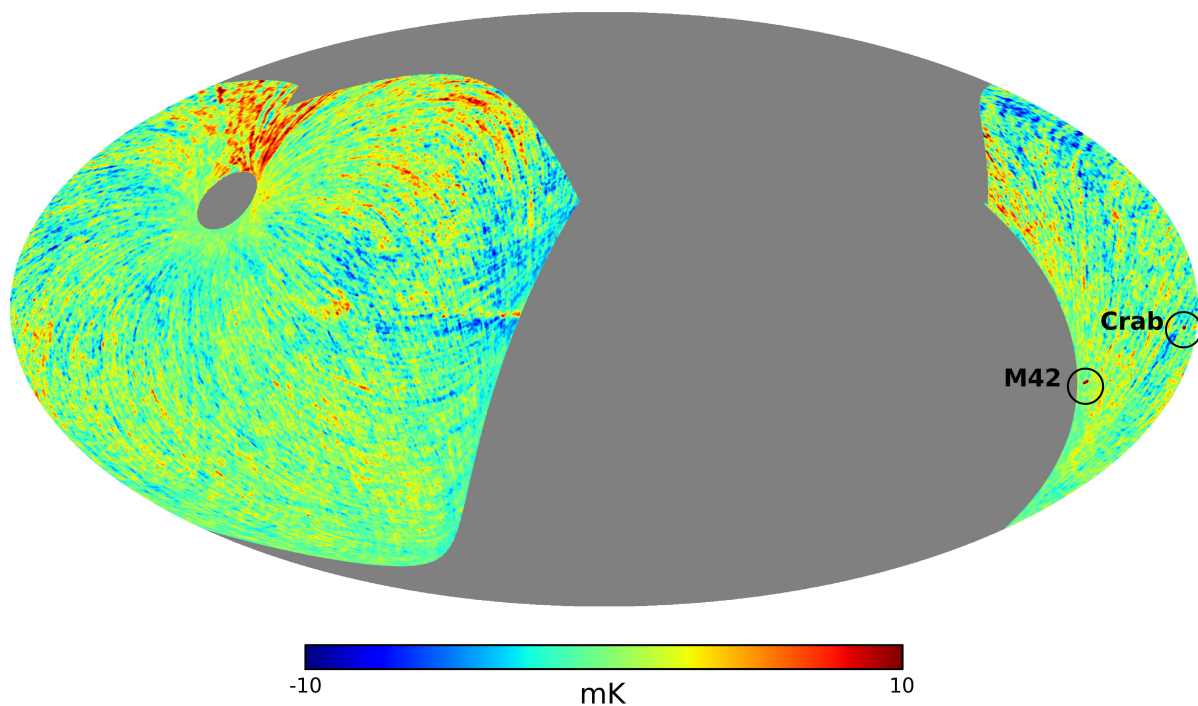
---

[9]`http://www.writelatex.com`

Figure 13: Mollweide projection of the B-Machine channel 6 *I* map after destriping in Galactic reference frame, smoothed with a 40′ gaussian beam. Galactic emission is visible toward the center of the map, compact sources M42 and the Crab Nebula are marked and labeled in the map. The equivalent map in Equatorial reference frame is presented in Fig 8c.

Balay, S., Gropp, W.D., McInnes, L.C., Smith, B.F., 1997. Efficient management of parallelism in object oriented numerical software libraries, in: Arge, E., Bruaset, A.M., Langtangen, H.P. (Eds.), Modern Software Tools in Scientific Computing, Birkhäuser Press. pp. 163–202.

Delabrouille, J., 1998. Analysis of the accuracy of a destriping method for future cosmic microwave background mapping with the PLANCK SURVEYOR satellite. AAPS 127, 555–567. doi:10.1051/aas:1998119.

Dobler, G., Finkbeiner, D.P., 2008. Extended Anomalous Foreground Emission in the WMAP Three-Year Data. APJ 680, 1222–1234. doi:10.1086/587862, arXiv:0712.1038.

Dupac, X., Tauber, J., 2005. Scanning strategy for mapping the Cosmic Microwave Background anisotropies with Planck. AAP 430, 363–371. doi:10.1051/0004-6361:20041526, arXiv:arXiv:astro-ph/0409405.

Efstathiou, G., 2005. Effects of destriping errors on estimates of the CMB power spectrum. MNRAS 356, 1549–1558. doi:10.1111/j.1365-2966.2004.08590.x, arXiv:arXiv:astro-ph/0407571.

Gabriel, E., Fagg, G.E., Bosilca, G., Angskun, T., Dongarra, J.J., Squyres, J.M., Sahay, V., Kambadur, P., Barrett, B., Lumsdaine, A., Castain, R.H., Daniel, D.J., Graham, R.L., Woodall, T.S., 2004. Open MPI: Goals, concept, and design of a next generation MPI implementation, in: Proceedings, 11th European PVM/MPI Users'

Group Meeting, Budapest, Hungary. pp. 97–104.

Gold, B., Odegard, N., Weiland, J.L., Hill, R.S., Kogut, A., Bennett, C.L., Hinshaw, G., Chen, X., Dunkley, J., Halpern, M., Jarosik, N., Komatsu, E., Larson, D., Limon, M., Meyer, S.S., Nolta, M.R., Page, L., Smith, K.M., Spergel, D.N., Tucker, G.S., Wollack, E., Wright, E.L., 2011. Seven-year Wilkinson Microwave Anisotropy Probe (WMAP) Observations: Galactic Foreground Emission. APJS 192, 15. doi:10.1088/0067-0049/192/2/15, arXiv:1001.4555.

Gorski, K.M., Hivon, E., Banday, A.J., Wandelt, B.D., Hansen, F.K., Reinecke, M., Bartelmann, M., 2005. Healpix: A framework for high-resolution discretization and fast analysis of data distributed on the sphere. The Astrophysical Journal 622, 759. URL: http://stacks.iop.org/0004-637X/622/i=2/a=759.

Haslam, C.G.T., Salter, C.J., Stoffel, H., Wilson, W.E., 1982. A 408 MHz all-sky continuum survey. II - The atlas of contour maps. AAPS 47, 1.

Heroux, M.A., Bartlett, R.A., Howle, V.E., Hoekstra, R.J., Hu, J.J., Kolda, T.G., Lehoucq, R.B., Long, K.R., Pawlowski, R.P., Phipps, E.T., Salinger, A.G., Thornquist, H.K., Tuminaro, R.S., Willenbring, J.M., Williams, A., Stanley, K.S., 2005. An overview of the trilinos project. ACM Trans. Math. Softw. 31, 397–423. doi:http://doi.acm.org/10.1145/1089014.1089021.

Keihänen, E., Keskitalo, R., Kurki-Suonio, H., Poutanen, T., Sirviö, A.S., 2010. Making cosmic microwave background temperature

and polarization maps with MADAM. AAP 510, A57. doi:10. 1051/0004-6361/200912813, arXiv:0907.0367.

King, O.G., Copley, C., Davies, R., Davis, R., Dickinson, C., Hafez, Y.A., Holler, C., John, J.J., Jonas, J.L., Jones, M.E., Leahy, J.P., Muchovej, S.J.C., Pearson, T.J., Readhead, A.C.S., Stevenson, M.A., Taylor, A.C., 2010. The C-Band All-Sky Survey: instrument design, status, and first-look data, in: Society of Photo-Optical Instrumentation Engineers (SPIE) Conference Series. doi:10.1117/ 12.858011, arXiv:1008.4082.

Kurki-Suonio, H., Keihänen, E., Keskitalo, R., Poutanen, T., Sirviö, A.S., Maino, D., Burigana, C., 2009. Destriping CMB temperature and polarization maps. AAP 506, 1511–1539. doi:10.1051/ 0004-6361/200912361, arXiv:0904.3623.

Maino, D., Burigana, C., Górski, K.M., Mandolesi, N., Bersanelli, M., 2002. Removing 1/f noise stripes in cosmic microwave background anisotropy observations. AAP 387, 356–365. doi:10.1051/ 0004-6361:20020242, arXiv:arXiv:astro-ph/0202271.

Maino, D., Burigana, C., Maltoni, M., Wandelt, B.D., Górski, K.M., Malaspina, M., Bersanelli, M., Mandolesi, N., Banday, A.J., Hivon, E., 1999. The Planck-LFI instrument: Analysis of the 1/f noise and implications for the scanning strategy. AAPS 140, 383–391. doi:10.1051/aas:1999429, arXiv:arXiv:astro-ph/9906010.

Natoli, P., de Gasperis, G., Gheller, C., Vittorio, N., 2001. A Map-Making algorithm for the Planck Surveyor. AAP 372, 346–356. doi:10.1051/0004-6361:20010393, arXiv:arXiv:astro-ph/0101252.

Planck Collaboration, 2013. Planck intermediate results. IX. Detection of the Galactic haze with Planck. AAP 554, A139. doi:10. 1051/0004-6361/201220271, arXiv:1208.5483.

Planck Collaboration, Ade, P.A.R., Aghanim, N., Armitage-Caplan, C., Arnaud, M., Ashdown, M., Atrio-Barandela, F., Aumont, J., Baccigalupi, C., Banday, A.J., et al., 2013. Planck 2013 results. XII. Component separation. ArXiv e-prints arXiv:1303.5072.

Planck Collaboration, Ade, P.A.R., Aghanim, N., Arnaud, M., Ashdown, M., Aumont, J., Baccigalupi, C., Balbi, A., Banday, A.J., Barreiro, R.B., et al., 2011. Planck early results. XX. New light on anomalous microwave emission from spinning dust grains. AAP 536, A20. doi:10.1051/0004-6361/201116470, arXiv:1101.2031.

Poutanen, T., de Gasperis, G., Hivon, E., Kurki-Suonio, H., Balbi, A., Borrill, J., Cantalupo, C., Doré, O., Keihänen, E., Lawrence, C.R., Maino, D., Natoli, P., Prunet, S., Stompor, R., Teyssier, R., 2006. Comparison of map-making algorithms for CMB experiments. AAP 449, 1311–1322. doi:10.1051/0004-6361: 20052845, arXiv:arXiv:astro-ph/0501504.

Revenu, B., Kim, A., Ansari, R., Couchot, F., Delabrouille, J., Kaplan, J., 2000. Destriping of polarized data in a CMB mission with a circular scanning strategy. AAPS 142, 499–509. doi:10.1051/ aas:2000308, arXiv:arXiv:astro-ph/9905163.

Saad, Y., Schultz, M.H., 1986. Gmres: A generalized minimal residual algorithm for solving nonsymmetric linear systems. SIAM Journal on scientific and statistical computing 7, 856–869.

Shewchuk, J.R., 1994. An introduction to the conjugate gradient method without the agonizing pain.

Spitzer Jr, L., 2008. Physical processes in the interstellar medium. Wiley. com.

The HDF Group, 2000-2010. Hierarchical data format version 5. URL: http://www.hdfgroup.org/HDF5.

Weiland, J.L., Odegard, N., Hill, R.S., Wollack, E., Hinshaw, G., Greason, M.R., Jarosik, N., Page, L., Bennett, C.L., Dunkley, J., Gold, B., Halpern, M., Kogut, A., Komatsu, E., Larson, D., Limon, M., Meyer, S.S., Nolta, M.R., Smith, K.M., Spergel, D.N., Tucker, G.S., Wright, E.L., 2011. Seven-year Wilkinson Microwave Anisotropy Probe (WMAP) Observations: Planets and Celestial Calibration Sources. APJS 192, 19. doi:10.1088/ 0067-0049/192/2/19, arXiv:1001.4731.

Williams, B., 2010. The B-Machine Polarimeter: A Telescope to Measure the Polarization of the Cosmic Microwave Background. Ph.D. thesis. University of California, Santa Barbara.

Wright, E.L., Smoot, G.F., Bennett, C.L., Lubin, P.M., 1994. Angular power spectrum of the microwave background anisotropy seen by the COBE differential microwave radiometer. APJ 436, 443–451. doi:10.1086/174919, arXiv:arXiv:astro-ph/9401015.

Zonca, A., . Bmachine 40ghz cmb polarimeter sky maps. URL: http: //dx.doi.org/10.6084/m9.figshare.644507.